This paper is accepted in International Journal of Heat and Mass Transfer

Thermal performance investigation in a novel corrugated plate heat exchanger

Salman Alzahrani[1,2], Mohammad S. Islam[1], Suvash C. Saha[1,*], Feng Xu[3]

[1]School of Mechanical and Mechatronic Engineering, University of Technology Sydney, Ultimo NSW 2007, Australia
[2]Department of Mechanical Engineering, Al baha University, Al baha, Saudi Arabia
[3]School of Civil Engineering, Beijing Jiaotong University, Beijing 100044, China

*Corresponding author: Email: suvash.saha@uts.edu.au, Tel:+ 61 2 9514 3183

Abstract

Compact heat exchangers have become an essential necessity for power production and multi other purposes on daily basis. The corrugated plate heat exchangers (PHEs) are well-known for their high thermal performance. This study proposes a unique PHE with a simple modification that can boost its thermal performance significantly. The overall tests have been conducted on four PHEs for two symmetric chevron angles (β) of 30°/30° and 60°/60°. Two PHEs belong to the newly PHEs, and the other two belong to the well-known basic PHE. Data are obtained for single-phase (water-water), counter-current arrangements, and for Reynolds number (Re) ranges from 500 to 2500. Sophisticated mesh techniques have been adopted to develop the mesh for the plates and the fluids between the plates. An appropriate grid refinement test has been carried out for the accuracy of the numerical results. The results have been validated with benchmark experimental and numerical data. A realizable $k-\varepsilon$ turbulence model with scalable wall treatment found to provide the most consistent and accurate prediction of the thermal performance of PHE. The numerical results showed that, the Nu and the effectiveness (ϵ) of the newly developed PHEs are much higher than that of the basic one, which can be very useful when a heavy heat duty is required. The enhancement for Nu is up to 75% and for ϵ is up to 42%, and generally both exhibit a direct proportional relationship with Re. Based on the numerical result, a new correlation to predict Nu has been developed.

Keywords: Corrugated plate heat exchanger; Thermal performance; Numerical modelling; Turbulent

1. Introduction

The use of PHEs has become an essential necessity on daily basis. PHE is the most efficient among other conventional type of heat exchangers (HEs). Many researchers have been

investigating new ways to enhance the heat transfer process in HEs [1-8], and other research conducted to optimize the performance for different types of the HEs [9-12]. PHEs are compact in nature, have high thermal effectiveness, and hence close approach temperatures (2 °C temperature difference) can be reached [13]. Therefore, PHEs are important particularly for heat recovery and regeneration applications. In addition, PHEs have modular nature that eases the cleaning process as well as making the system flexible, by adding or removing plates to meet the energy requirements quickly. PHEs have been employed in food, paper/pulp, power, pharmaceutical industries, HVAC and many other applications [14, 15]. In PHEs, the turbulence flow can be achieved at low Re, $\mathrm{Re} > 400$ [16, 17]. In addition, PHEs are lighter and require less space. Troup et al [18] performed one of the earliest studies on PHE performance, who considered washboard plate type HE. However, later the chevron plate has become the most popular due to its high thermal performance among other plate types (e.g. wavy, and zig-zag plate). The impact of different β on PHE's thermal performance was investigated by Okada et al [19], where the β was considered with respect to the horizontal centreline. However, it is more common that β to be considered with respect to the longitudinal centreline as shown in Fig.1. Later Manglik et al [20] studied heat transfer characteristics (HTC) in PHE for $\beta = 30°/30°$, 60°/60° and 30°/60°. The correlations for the whole study were incorporated in one formula. Nevertheless, each correlation should be separately reported, in order to be able to test the agreement between each β correlation and the general formula. One-one pass, water-water fluids for the same β have been tested by Ayub [21]. An equal heat transfer coefficient (h) and Nu were considered for the both sides as the Reynolds number was the same at the cold and at the hot side. The same Re on the both sides of the PHE does not imply h will be the same, as h depends on many other factors i.e. fluid viscosity, fluid density, fluid velocity and many other parameters. For the cold side, h is likely greater than that of hot side, because thermal boundary layer resistance is lower in case of cold fluids [22]. In addition, heat capacity rate (C) of cold water is higher than that of hot water as the viscosity of cold water is higher than that of hot water. Hence the velocity of the cold water would be higher in order to meet the same Re, and consequently the mass flow rate of cold water will be higher than that of hot water. Therefore, considering Nu as the same on both sides is not an accurate assumption. Similar studies performed on PHE to investigate the impact of different chevron angles [4, 6, 23-33]. The experimental and numerical studies have concluded that the flow inside the PHE is non-uniform and tends to flow toward the lateral edges of the plate [34]. However, the study did not consider the thermal performance of PHEs. Kanaris [35] carried out both experimental and numerical studies about thermo-hydraulic characteristics in PHE with one corrugated plate ($\beta = 60°$). The study used one corrugated plate, while the other plate was flat. The port effect and the pressure drop were ignored. In fact, to be able to study heat transfer inside the PHE, at least three plates should be considered (two channels) to allow heat transfer process to take place. One year later, Kanaris [36] executed another numerical investigation using CFD, a three plates were generated with $\beta = 60°$. The shape of the corrugation they considered was trapezoidal. The real corrugation however is sinusoidal shape. Also, the port effect was neglected again.

A numerical study for PHE with two channels was performed by Tsai et al [37]. The flow maldistribution was investigated by applying Bassiouny and Martin formula [38, 39]. The heat

transfer was ignored, and the range of Reynolds number was small ($Re \leq 1700$). A two symmetric $\beta = 30°/30°$ and 60°/60° PHEs were numerically studied using CFD by Asif [40]. The thermo-hydraulic characteristics was investigated in the form of Nusselt number. An essential detail was not provided for supporting the appropriateness of adopting the turbulence model, and no information of the number of channels or plates. The Wilson plot technique was applied in their numerical study. However, a comprehensive understanding of CFD would help to avoid going through this long iterative process. The good thing of considering CFD study is that it enables the user to find the temperature at any spot on the model, and the average temperature for any side of the plate. Consequently h can directly be calculated from numerical data. This would be very hard to get from an experimental model. In all previous numerical studies reviewed in this study, the mesh dependency tests were not provided. In addition, the mesh statistics was also insufficient. Alzahrani et al [22] numerically investigated the effect of Prandtl number (Pr) on heat transfer and friction factor (*f*), by conducting two sets of tests at hot fluid side, while the cold water kept at the cold side for all cases. First set was for hot air, and the second set was for hot water. The result concluded that, both Nu and *f* increase as Pr increases.

Most research either studied the impact of different β on heat transfer characteristics or studied the fluid flow pattern inside PHE's channels. However, in order to be able to reduce its size and make the system more compact, there is a large number of ongoing efforts to find new techniques to enhance the performance of the heat exchanger. In general, heat transfer enhancement methods are active, passive, and compound. Active technique requires an external power for the enhancement such as induced pulsation, and surface vibration. Passive technique involves a geometrical modification to the fluid flow passage, or using inserts in the flow passage, or both. An example for passive technique is inserting twisted tape to promote turbulence flow regime, adding fins, and extending surface. In compound method, both active and passive techniques are used. In general, passive technique is the preferred one [41], because the potential of active technique is limited due to the design complexity [42]. Therefore, the present study introduces a new modification in PHE flow mechanism as described in the following section, which could enhance convective heat transfer significantly between the cold and hot fluids, and consequently the fuel consumption can be reduced [43]. The numerical thermo-hydraulic performance tests carried out on counter-current flow arrangement, and for two symmetric $\beta = 30°/30°, \text{and } 60°/60°$. Nu is employed as an indicator for heat transfer improvement, and PHE effectiveness (ϵ) is employed to compare the thermal performance between the basic and the new PHE design. The PHE comprised of four channels (five plates), two of them are pertaining to the cold side, which represent the utility fluid, and the other two pertaining to the hot side, which represent the product fluid. Therefore, the present study is performed on the hot side of PHE. The port effect, and the corrugations shape have been considered for all cases in order to get as closer as possible to simulate thermal-hydraulic performance in real PHE.

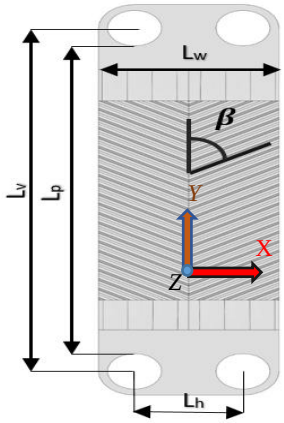

Fig.1. Geometrical parameter illustration for chevron plate type.

2. The new PHE design approach

The material technology of PHE has been constantly improved, which allows the usage of PHE for further applications such as chemical processes. In addition, the brazed PHE has been introduced in order to resist higher pressures and temperatures. However, the basic design of PHE has not been changed a lot since it was invented in the 1920s. All studies of the PHEs were to test the performance, flow patterns inside the PHE, or to study the effect of a specific parameter. In the basic design, PHE's thermal performance is high. However, the current study introduces a new modification in the basic design that improves the PHE's thermal performance significantly. The modification implies more degree of control of the fluid flow on the plate's surface. However, the fluid is distributed on the plate's surface randomly in the basic design.

In the basic and new PHEs, the gasket is used to regulate the fluid directions through the PHE. The design of the new gasket shown in Fig. 2, where the separator has been installed at the middle of the plate for two reasons. Firstly, it guides the fluid to the desired direction. Secondly, it replaces the contact points at the middle between every two consecutive plates, where the heat transfer magnitude is negligible at this area [44]. In addition, it also assures equal fluid distribution on each plate side.

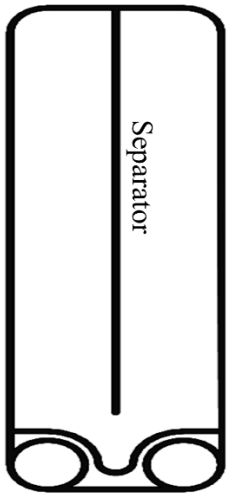

Fig. 2: The current gasket design

The flow mechanism in the new PHE is as following; the hot fluid is flowing from bottom to top and then from top to bottom. At the same time on the adjacent plate, the cold fluid is flowing in the opposite direction with respect to the hot fluid as shown in Fig. 3 (b). In all well-known PHEs configurations, the fluid enters from one side and exits from the opposite side either vertically (as shown in Fig. 3(a)) or diagonally. However, in the new design, the fluid enters and leaves from the port on the same side, in order to maximize the amount of heat recovery (reducing temperature gradient) between the cold and the hot fluids, and consequently enhancing PHE's thermal performance.

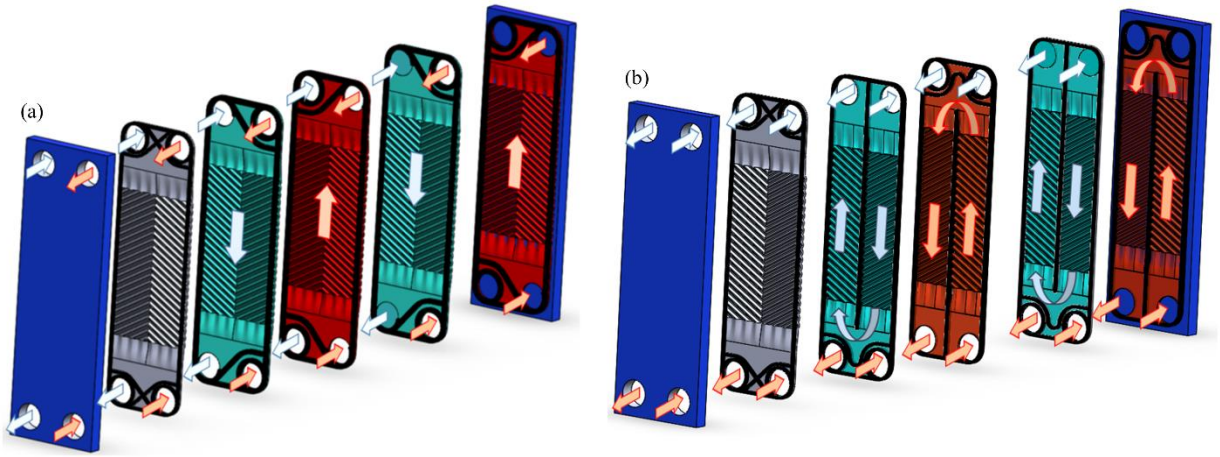

Fig. 3: Illustrative schematics of, (a) flow arrangement for 1-1 pass in the basic PHE, and (b) The current flow mechanism

3. Numerical method

3.1 Governing equations

Fluids inside PHE are subjected to turbulent flow due to the change in velocity in the corrugations for the Reynolds number considered here. In addition, heat transfer takes place between cold and hot sides, and consequently a transition of physical properties occurs such as temperature, pressure, viscosity, density, and velocity. Therefore, Navier-Stockes Eq. (NS) (1) is used to estimate changes on these properties during the thermal and dynamic interaction as shown below:

$$\frac{\partial}{\partial x_j}(\rho u_i u_j) = -\frac{\partial p}{\partial x_i} + \frac{\partial}{\partial x_j} + \left[(\mu + \mu_t)\frac{\partial u_i}{\partial x_j}\right] \quad (1)$$

NS can be considered as Newton's second law applied to the fluid motion. Inertia, pressure, and viscous forces are estimated. ANSYS FLUENT 19.0 solves these equations along with continuity Eq. (2). Whereas NS refers to conservation of momentum, and continuity equation refers to conservation of mass.

$$\frac{\partial}{\partial x_i}(\rho u_i) = 0 \quad (2)$$

In addition, the energy equation is included to resolve heat transfer among the cold fluid, the hot fluid, and the plates as shown in Eq. (3):

$$\rho C_p \frac{\partial}{\partial x_j}(u_j T) = k_{eff}\frac{\partial^2 T}{\partial x_j^2} + (T_{ij})_{eff}\frac{\partial u_i}{\partial x_j} \quad (3)$$

3.2 Turbulence model

Up today, there is no single or favorite turbulence model that can be applied for any turbulence flow modelling. ANSYS FLUENT provides a large selection of turbulence models, however, care must be taken during choosing an appropriate model. One of the most common turbulence model that is considered as an industry standard model is $k-\varepsilon$ model [45]. The turbulence kinetic energy, k represents the diversity of fluid fluctuations. The turbulence eddy dissipation, ε represents the dissipation rate of the velocity fluctuations. On the other hand, the shear stress transport (SST) $k-\omega$ turbulence model is also used to simulate some heat transfer processes [46, 47]. Whereas ω represents the dissipation rate between ε to k. The two equations turbulence models, $k-\varepsilon$ and $k-\omega$ differs from each other. The SST $k-\omega$ model is the combination of $k-\omega$ and standard $k-\varepsilon$. Also, the SST $k-\omega$ model can resolve the boundary layers near the wall, whereas, the standard $k-\varepsilon$ model can resolve the boundary layer away from the wall. Therefore, the standard $k-\varepsilon$ model is not suitable for most applications due to the incompetency of standard approach. The realizable $k-\varepsilon$ model is relatively new approach that differs from standard one. A new formulation approach for the calculation of eddy viscosity μ_t (4) (also called turbulent viscosity) has been developed, where C_μ is no longer constant.

$$\mu_t = \rho\, C_\mu \frac{k^2}{\varepsilon} \tag{4}$$

The transport Eqs. (5) and (6) are used to obtain the turbulence kinetic energy k, and the dissipation rate ε values, respectively.

$$\frac{\partial}{\partial t}(\rho k) + \frac{\partial}{\partial x_i}(\rho k u_i) = \frac{\partial}{\partial x_j}\left[\left(\mu + \frac{\mu_t}{\partial k}\right)\frac{\partial k}{\partial x_j}\right] + G_k + G_b - \rho\varepsilon - Y_M + S_k \tag{5}$$

$$\frac{\partial}{\partial t}(\rho\varepsilon) + \frac{\partial}{\partial x_i}(\rho\varepsilon u_i) = \frac{\partial}{\partial x_j}\left[\left(\mu + \frac{\mu_t}{\partial \varepsilon}\right)\frac{\partial \varepsilon}{\partial x_j}\right] + C_{1\varepsilon}\frac{\varepsilon}{k}(G_k + C_{3\varepsilon}G_b) - C_{2\varepsilon}\,\rho\frac{\varepsilon^2}{k} + S_\varepsilon \tag{5}$$

where G_k and G_b characterize the generation of k due to the mean velocity gradient and buoyancy, respectively. Y_M depicts the addition of fluctuating enlargement in compressible turbulence to the total dissipation. $C_{1\varepsilon}, C_{2\varepsilon}$, and $C_{3\varepsilon}$ are constants. ∂k, and $\partial \varepsilon$ characterize the turbulence Prandtl numbers for turbulence kinetic energy k, and its dissipation ε, respectively. User-define source terms S_k and S_ε can be implemented when needed.

A realizable $k-\varepsilon$ model satisfies a specific mathematical constraint as well as complied with turbulent flow physics. The spreading rate of planar and round jet can accurately be predicted. In addition, a realizable $k-\varepsilon$ model can provide a superior performance for simulating complex flows, that includes boundary layer reattachment, circulation, rotation, and strong adverse pressure gradient. Both $k-\varepsilon$ and $k-\omega$ are y^+ independent. However, adopting the most appropriate near wall function depends on the degree of mesh refinement near the wall. Near wall treatment methods are very useful when the prism boundary layers are not sufficient to resolve those layers. Standard wall treatment denotes that, the whole boundary layer mesh is located within the log-law region. However, for engineering applications, this is difficult to be fulfilled. That is because of existing of different geometrical scales as well as arbitrary refinement, especially for geometries that contain narrow curves and passages. Enhanced and non-equilibrium wall functions can be adopted for ε based. However, the mesh resolution should be high, which is computationally expensive. Altogether, both enhanced and non-equilibrium approaches are not recommended if viscous sub-layer region is the area of interest. Instead SST $k-\omega$ can perform better in this region [45].

On the other hand, scalable wall function introduces an elegant solution for the issue of arbitrary refinement. Particularly in complicated geometries. The mesh is virtually shifted to the log-law region ($y^+ \approx 11.225$). Hence the invalid modelling of the laminar sub-layer and buffer region is avoided.

Generally, all turbulence models have been tested for this problem. The realizable $k-\varepsilon$ model with scalable wall function has been adopted. Because it showed the most accurate result that is close to the experimental one as well as its consistency with different Re.

3.3 Data formulation

In the current study, Re set as the same for both cold and hot fluids inside PHE's channels. However, Nu was not considered to be the same.

$$Re = \frac{\dot{m}\, d_e}{\mu\, A_\circ\, N} \tag{6}$$

$Re, \mu, A_\circ, N$, and d_e are known, $\dot{m}$ is calculated to meet the required Re. d_e is twice the plate's corrugation depth.

The essential measurements are the outlet temperatures of cold and hot fluids, and the hot walls temperature. The fluids' inlet temperatures and velocities have been set in the initial conditions. Two main non-dimensional parameters have been employed to express heat transfer data. Nu is used to a scale heat transfer improvement, and ϵ is calculated to compare the enhancement in thermal performance between the new and the basic PHEs for two symmetric β = 30°/30°, and 60°/60°. The hot side of PHE is considered as the product fluid, while the cold side is considered as the utility fluid. Therefore, Nu, and ϵ are considered for the hot side. Nu is given by:

$$Nu = \frac{h_h d_e}{k} \tag{7}$$

The heat transfer coefficient, h_h is calculated as follows:

$$Q_h = \dot{m}_h c_{p,h}\left(T_{h,i} - T_{h,o}\right) \tag{8}$$

$c_{p,h}$ has been extracted from the tables of thermodynamics at hot fluid bulk mean temperature as follows:

$$T_{h,b} = \frac{(T_{h,i} + T_{h,o})}{2} \tag{9}$$

Note, Q_c is calculated from Eq. (11) below. $c_{p,c}$ is also extracted at the bulk mean cold fluid temperature as shown in Eq. (12) below. The difference between Q_h and Q_c should always be zero to fulfil the energy balance. However, the difference of about 95% of the simulations is less than $\pm$ 2%, and $\pm$4-6% for the rest of the simulations. Therefore, Q_{avg} is taken as the average value of the hot and cold heat load and considered for the current calculations.

$$Q_c = \dot{m}_c c_{p,c}\left(T_{c,o} - T_{c,i}\right) \tag{10}$$

$$T_{c,b} = \frac{(T_{c,i} + T_{c,o})}{2}. \tag{11}$$

Now Q_{avg} is known, and h_h is given by:

$$h_h = \frac{Q_{avg}}{A(T_{h,b} - T_{w,h})} \tag{13}$$

Q_{max} is the maximum possible amount of heat that could be exchanged between hot and cold fluids and is given by:

$$Q_{max} = C_{min}(T_{h,i} - T_{c,i}) \tag{14}$$

C_{min} is the minimum heat capacity. For all cases in the current study $C_h < C_c$:

$$\begin{aligned} C_h &= \dot{m}_h c_{p,h} \\ C_c &= \dot{m}_c c_{p,c} \end{aligned} \tag{15}$$

Then, ϵ is determined as follows:

$$\epsilon = \frac{Q_{avg}}{Q_{max}} \tag{12}$$

4. Model setup

4.1 CAD geometry creation

Four PHEs are drawn by using Solidworks CAD 2016. Two symmetric PHEs with $\beta = 30°/30°$, and $60°/60°$ are developed according to PHE's basic design. The other two symmetric PHEs with $\beta = 30°/30°$, and $60°/60°$ are drawn according to the new design criteria. Each PHE consists of five plates, which generate four channels. Two channels belong to the cold side and the other two belong to the hot side. All PHE's geometric parameters have been developed carefully. The corrugations have a sinusoidal shape similar to that one in real PHE. The port effect is considered. The hot port is created and merged with the hot side, and same is developed for the cold port side for both basic and new design PHEs.

4.2 Mesh optimization

A corrugated PHE contains a large number of curved and tilted narrow passages. Therefore, in order to ensure a sufficient mesh element in these narrow passages, an unstructured tetrahedron mesh elements are adopted. An advance technique has been employed to get a good quality mesh. Patch conforming and patch independent algorithms have been adopted simultaneously for the same geometry. The patch conforming is a Delaunay [48] mesher, where mesh refinement is carried out by using an advancing front point insertion technique. The meshing process uses the bottom up approach, meshing edges, faces, and volume in sequence. In patch conforming algorithm, excluding the de-featuring tolerance, all faces, and their boundaries are conformed. On the other hand, patch independent algorithm is based on spatial subdivision. The mesh refinement is carried out where necessary, particularly in holes, curves, and narrow passages. Large mesh elements are developed where possible such as on flat surfaces. Hence, one should look into covering the important complicated areas on the

geometry and allowing for faster computation at the same time. The meshing process uses top down approach. The volume mesh is carried out first, and then the surface mesh is created by projecting the volume mesh on to faces and edges. Samples of the mesh is shown in Fig. 4(a) and (b). To ensure solution stability, the mesh dependency tests have been carried out for each PHE as shown in Table 1. Mesh elements of 53.1 and 73 million for $\beta = 30°/30°$, for basic and new design PHEs have been adopted, respectively. Mesh elements of 14.8 and 16.1 million for $\beta = 60°/60°$, for basic and new design PHEs have been adopted, respectively.

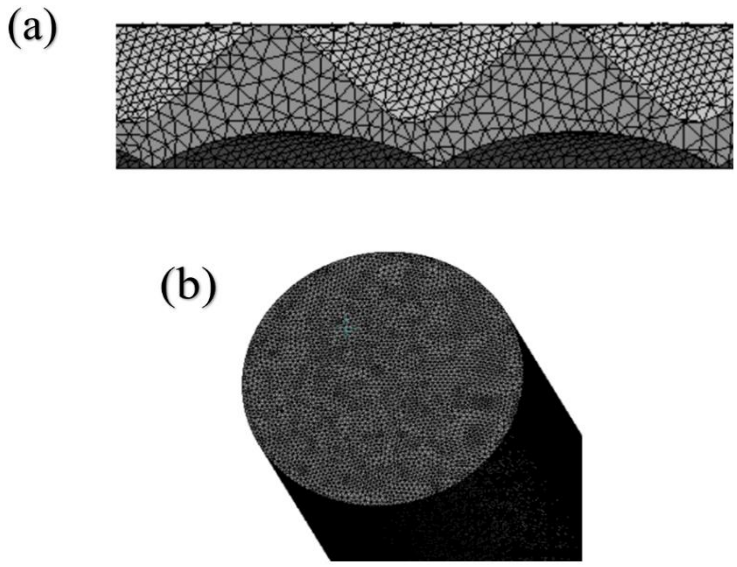

Fig. 4. (a) A side view for one corrugation mesh (The whole mesh is not visible due to the high-density elements), and (b) Close front view for mesh at the cold inlet port.

4.3 Boundary conditions and material properties specification

Both hot and cold fluids inlet boundary conditions are set as velocity inlet. The mass flow rate ($\dot{m}$) is calculated from Eq. (7) to meet the required Re value. Thus, velocity at the inlet can be calculated from $\dot{m}$. The working fluid is (water-water). The hot and the cold inlet water temperatures are set to 40 °C and 18°C respectively. The fluid's thermodynamics properties ($\rho, c_p, k_f,$ and μ) have been set for each fluid according to its temperature. Zero gauge pressure has been set at both cold and hot ports outlets. According to Ansys FLUENT user manual [45], the optimum value for turbulence intensity for the current flow pattern is 5%. The conjugate heat transfer is enabled, where the plate thickness is set to 0.5 mm. Stationary and no slip boundary conditions are set for all walls. Since almost all studies performed on PHEs have used stainless steel, and to be able to validate the numerical study, stainless steel is defined as the plate's material. The plate's ρ, c_p, and k are 8030 kg/m^3, 502.48 $J/kg.k$, and 16.27 $W/m.k$, respectively. All simulations are carried out on a high performance computing cluster using nodes with 3.3 GHz (28 cores) processor, and with 128 GB of RAM. For the mesh that contains 14.8 and 16.1 million element, the simulation time is approximately10-13 hours. For the mesh that contains 53.1 and 73 million elements, the time for each simulation is approximately 48-55 hours.

Table 1. Mesh independent test for basic (PHE^1) and new (PHE^2) PHEs.

	Mesh elements (million)	Outlet cold average temperature (K)	Outlet hot average temperature (K)
PHE^1 β =30°/30°	44	295.44	305.32
	53.1	295.75	305.82
	62	295.79	305.84
PHE^2 β =30°/30°	56.6	296.57	303.98
	73	296.78	304.02
	80	296.79	304.01
PHE^1 β =60°/60°	8	293.62	308.45
	14.8	293.95	308.85
	32	293.89	308.87
PHE^2 β =60°/60°	9.5	296.59	303.92
	16	296.75	303.82
	47	296.73	303.82

4.4 Model validation

The present study has been comprehensively validated with available experimental and CFD studies. The same working fluids and PHE's material from the available literatures are used in this study. The CFD study compared the Nu empirical correlation data with the published Nu empirical results for different β. Fig. 5(a) shows the empirical Nu deviation for $\beta = 60°/60°$. The maximum and the minimum deviations are found + 9% and +6% respectively with the findings of Okada et al [19]. The findings of the CFD study also compared with the measurement obtained by Gherasim et al [49] and Thonon et al [50], and the numerical results show good agreement with the published literatures. The findings of the present study have also been compared with the results of Muely et al. [20] and Lee et al [51], and found a negligible deviation with the published data. In case of $\beta = 30°/30°$, as shown in Fig. 5(b), the maximum and the minimum deviation with the study of Muely et al. [20] are +6% and +2% respectively. The maximum and the minimum deviation are found -9% and -4% respectively with the findings of Okada et al [19]. The maximum and the minimum deviation compared with Lee et al [51] are -4.7% and +1.3%, respectively. The numerical correlations of the present study for both $\beta = 30°/30°$ and $60°/60°$ are in the range of all other published correlations and shows an increasing trend. Many reasons could contribute in the deviation between the results. Some studies calculated average Nu between the cold and the hot sides of the PHE's [19] . Muely et al. [20] calculated Nu for the hot side, hence the current results are very close to this one.

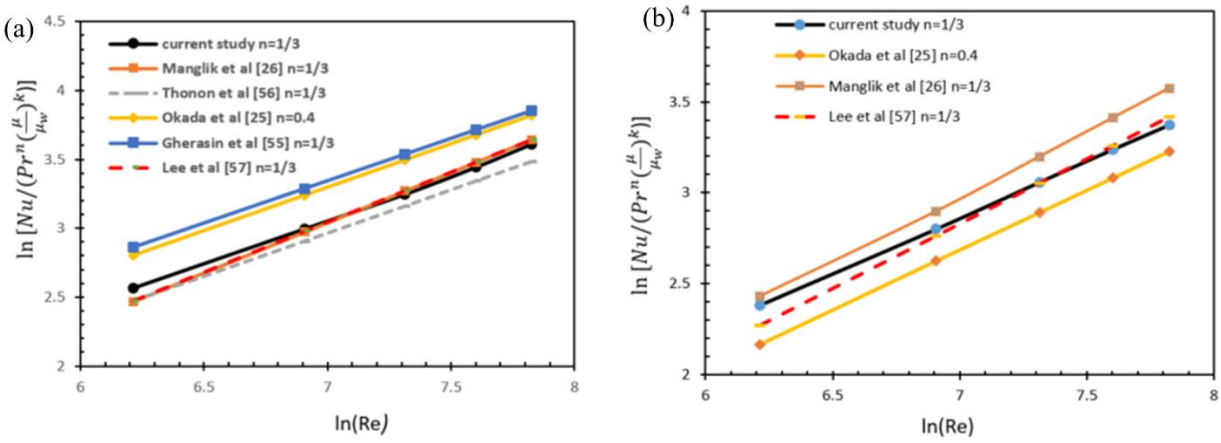

Fig. 5: Comparison of present Nu data with other experimental and numerical studies, (a) for $\beta = 60°/60°$, and (b) for $\beta = 30°/30°$.

Janusz et al [52] have tested a number of published correlations for better accuracy of the calculated Nu and reported that Muely et al. [20] correlation can predict Nu values reasonably well. Furthermore, the differences in the geometrical dimensions such as corrugation depth, aspect ratio (A_r), and even a small difference in the corrugation roundness may result in change in Nu values up to 18% [53]. However, the maximum deviation is always $\leq \pm 10\%$ except one case the maximum deviation is 11%. The calculated Nu of the present study shows good agreement with the published literature, which sufficiently indicate that present CFD model is accurate to predict the thermal performance of the corrugated PHE's.

5. Results and discussion

In the present study, four symmetric PHEs have been employed. Two of them are belonging to the well-known basic design with $\beta = 30°/30°$, and $60°/60°$. The other two are based on the new design criteria with the same chevron angle of $\beta = 30°/30°$, and $60°/60°$. The numerical simulations have been carried out for the single phase (water-water). All four PHEs have an identical geometrical dimension ($b, d_e, \beta,$ and A_r) and physical conditions ($T_{h,i} T_{c,i}$, and Re). Reynolds number ranges from 500 to 2500. Nusselt number has been calculated for all PHEs as shown in Fig. 6. The results show that, Nu is directly proportional to the plate's chevron angle as well as to the Re. In addition, the new design exhibits significant heat transfer enhancement for all cases. At the same Reynolds number, Nusselt number for the new PHE increases up to 75% compare to the basic PHE as shown in Table 2.

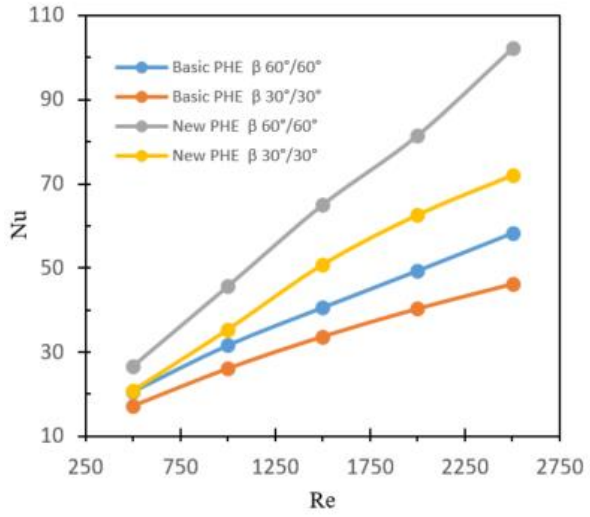

Fig. 6. Nu values versus Re for novel and basic PHEs.

The non-uniformity of the PHE's surfaces causes velocity fluctuation. The fluid has the maximum velocity at the corrugation's ridge and the minimum velocity at the corrugation's furrows as shown in Fig. 7. This fluctuation of velocity causes disruption, boundary layer re-attachment, and secondary flow development. Consequently, provide heat transfer enhancement.

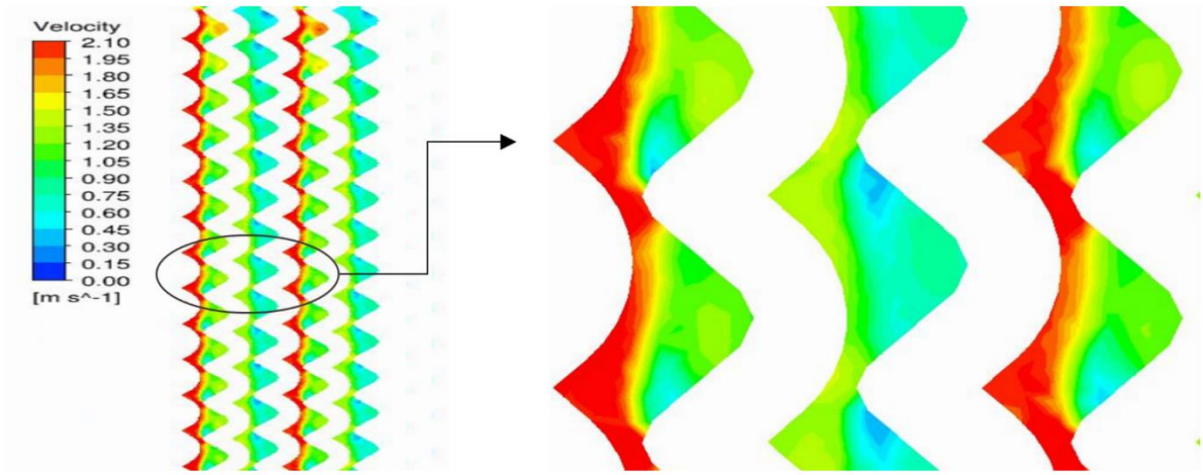

Fig. 7. ZY plane (side view) illustrates fluids velocity contour inside new PHE's channels with β 30°/30° at Re = 500

The longitudinal vortices in the corrugation's furrows are observed by [54]. In addition, Won et al [55] has carried out an instantaneous visualization of fluid flow inside the channel. The result showed a strong spanwise secondary flow, that moved in an opposite direction in the bottom and the top halves. The boundary layer re-attachment, and its rule in heat transfer augmentation was also confirmed by [56].

In the case of new PHE, Fig. 9. shows that, the Re varies significantly over the plate as the fluid is forced to flow along the specified half of the plate. The fluid velocity is about 3 times

higher than that of the basic PHE. Thus, more turbulent flow is developed, which would contribute in heat transfer augmentation. Fig. 8. shows the velocity contour inside the basic PHE. For the same mass flow rate, the fluid velocity is lower than that of the new one. Because in basic PHE the fluid flows and distributes randomly over the plate.

Table 2: Comparison between Nu of the basic (PHE^1) and the new (PHE^2) PHEs.

Re	**Nu PHE^1 60°/60°**	**Nu PHE^2 60°/60°**	**I %**	**Nu PHE^1 30°/30°**	**Nu PHE^2 30°/30°**	**I %**
500	20.6	26.7	29.8	17.1	20.9	22
1000	31.6	45.7	44.6	26	35.4	35.9
1500	40.6	65.1	60.2	33.7	50.8	50.9
2000	49.4	81.5	65.1	40.3	62.6	55.3
2500	58.3	102.2	75.3	46.2	72	56

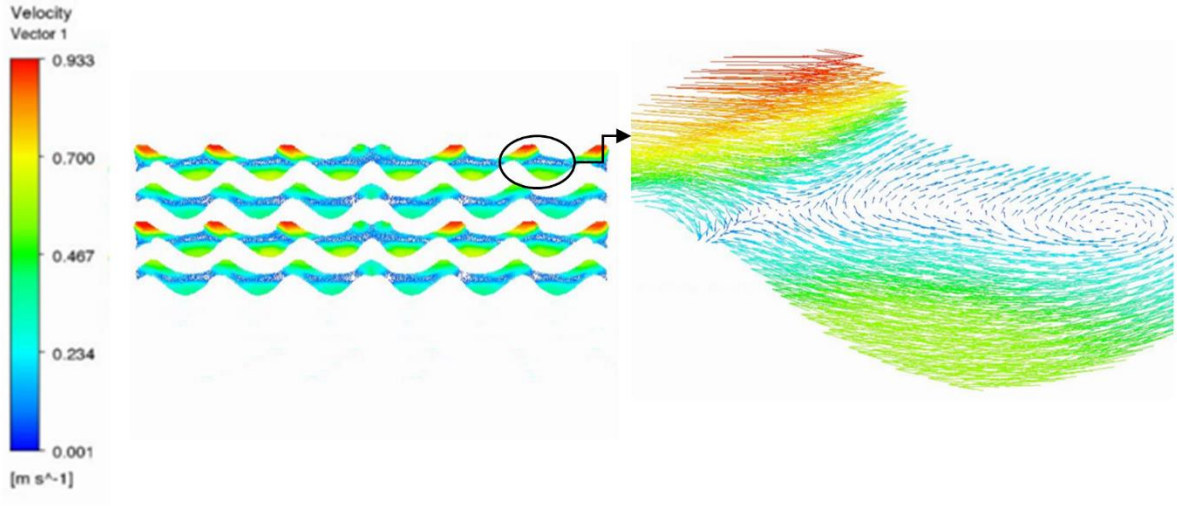

Fig. 8. ZX plane (Top view) for velocity vectors for basic PHE with β 60°/60° at Re = 500

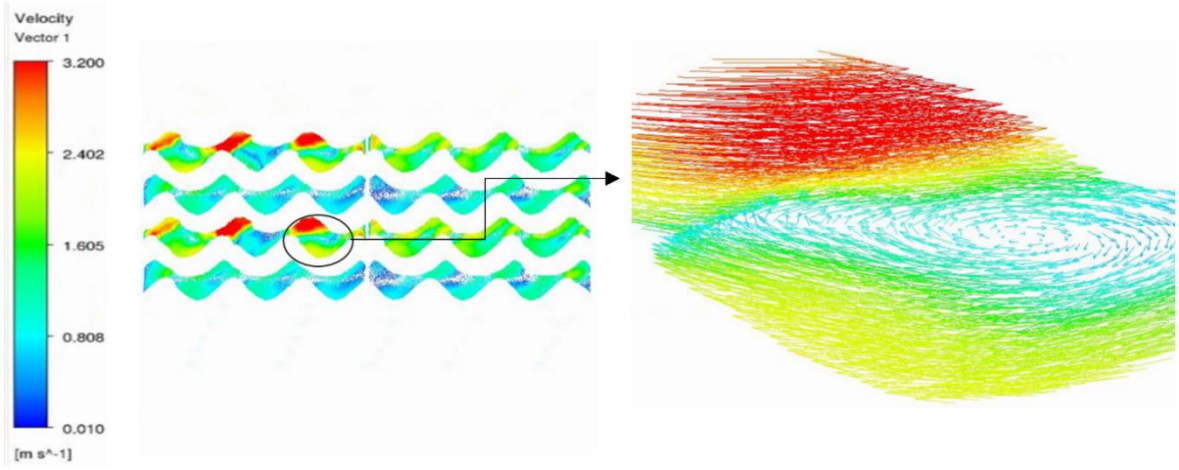

Fig. 9. ZX plane (Top view) for velocity vectors for new PHE with β 60°/60° at Re = 500

Thermal performance of basic and new PHEs has been calculated in the form of PHE's ϵ. Fig. 10 shows the PHE's ϵ versus Reynold number for all cases. In addition, the enhancement percentage for the new PHE's ϵ comparing with the ϵ of the basic one is given in Table 3.

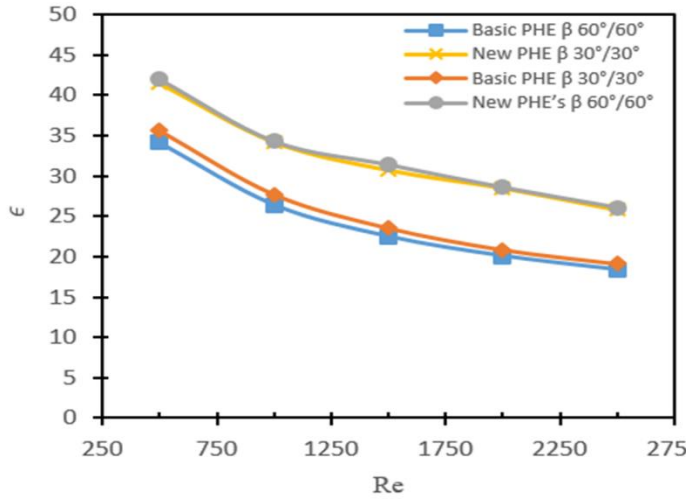

Fig. 10. Comparison between the ϵ of new and basic PHEs versus Re.

Table 3: Comparison between ϵ of the basic (PHE[1]) and the new (PHE[2]) PHEs.

Re	ϵ PHE[1] 60°/60°	ϵ PHE[2] 60°/60°	I %	ϵ PHE[1] 30°/30°	ϵ PHE[2] 30°/30°	I %
500	34.1	42	23	35.6	41.5	16.6
1000	26.4	34.3	30	27.7	34.2	23.5
1500	22.5	31.4	39.6	23.5	30.7	30.6
2000	20	28.6	42.5	20.8	28.5	36.8
2500	18	26.1	42.2	18.7	25.8	38

Fig. 11(a,b) and Fig. 12 (a,b) show temperature contour and profile on the hot channel that locates at the middle (as also shown in Fig.13.) of the new and the basic PHE, respectively. In the case of new PHE, the hot fluid's temperature decreasing rate is higher than that of the basic one. In addition, the hot fluid's temperature is more homogeneous. While in the case of basic PHE, the hot fluid's temperature shows less homogeneity. The temperature of the hot fluid on the left side is lower than that on the right side. That is because the cold fluid is entering from the left side in the fore and next adjacent cold channel as shown in Fig. 13.

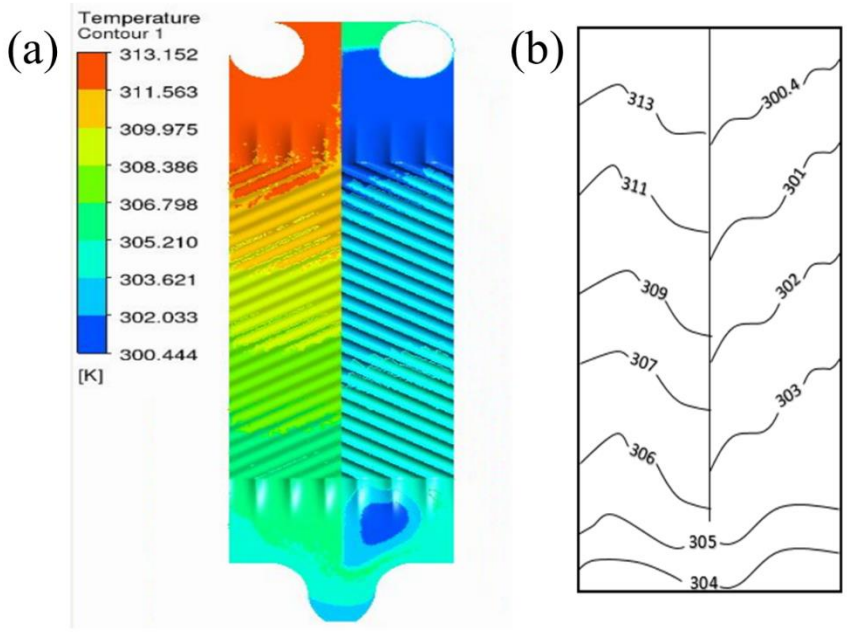

Fig. 11: For $\beta = 60°/60°$, and $Re = 500$ (a) temperature contour for new PHE, and (b) temperature profile for new PHE.

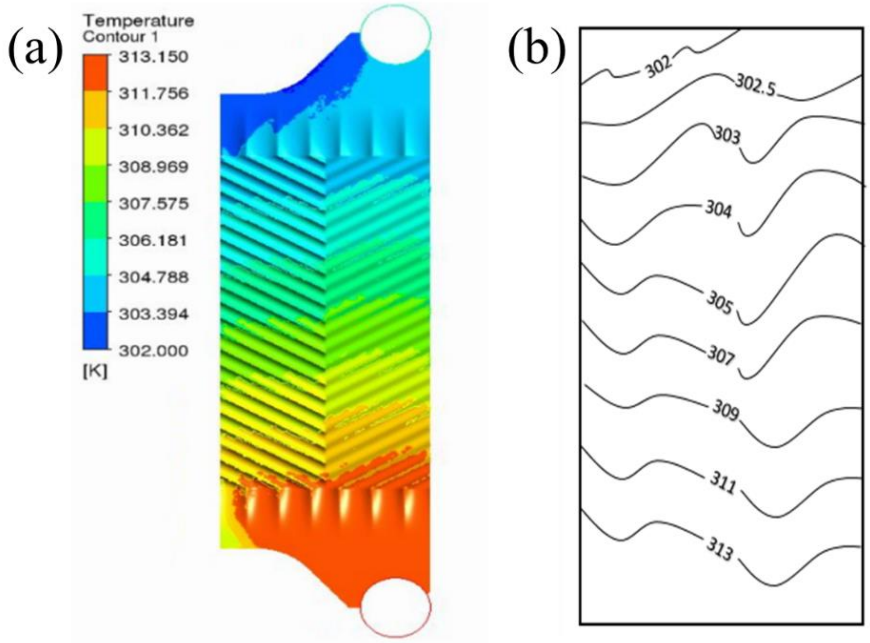

Fig. 12: For $\beta = 60°/60°$, and $Re = 500$ (a) temperature contour for basic PHE, and (b) temperature profile for basic PHE.

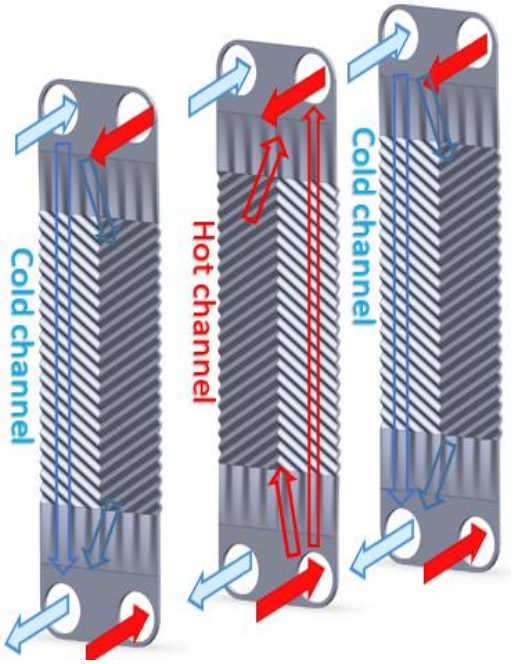

Fig. 13. Illustrative schematic for fluid flow arrangement in basic PHE

The temperature trend throughout the port of hot channel outlet as shown in Fig. 14 is presented in Fig. 15 (a) and (b). For all cases, the temperature of the last hot channel is higher than that of the first hot channel. Whereas, the last hot channel transfers heat with cold fluid from one side only (the side that locates just before the last channel).

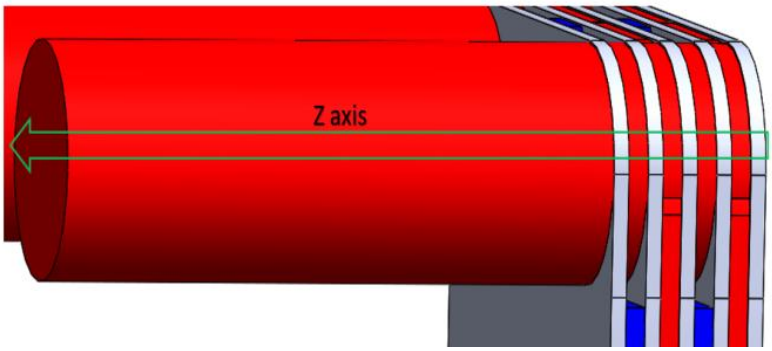

Fig. 14. Illustrative sketch for hot channel outlet port.

The first hot channel transfers heat with cold channels from the front and the back sides. Therefore, its temperature is always less than the hot channel that locates at the end. All 4 trends at the beginning show descending in temperature as hot fluid moves through z axis. Because, the hot fluid of the last channel mixes with the hot fluid of the first channel, which has lower temperature, the temperature increases up to a specific limit, allowing for the temperature balance to take place.

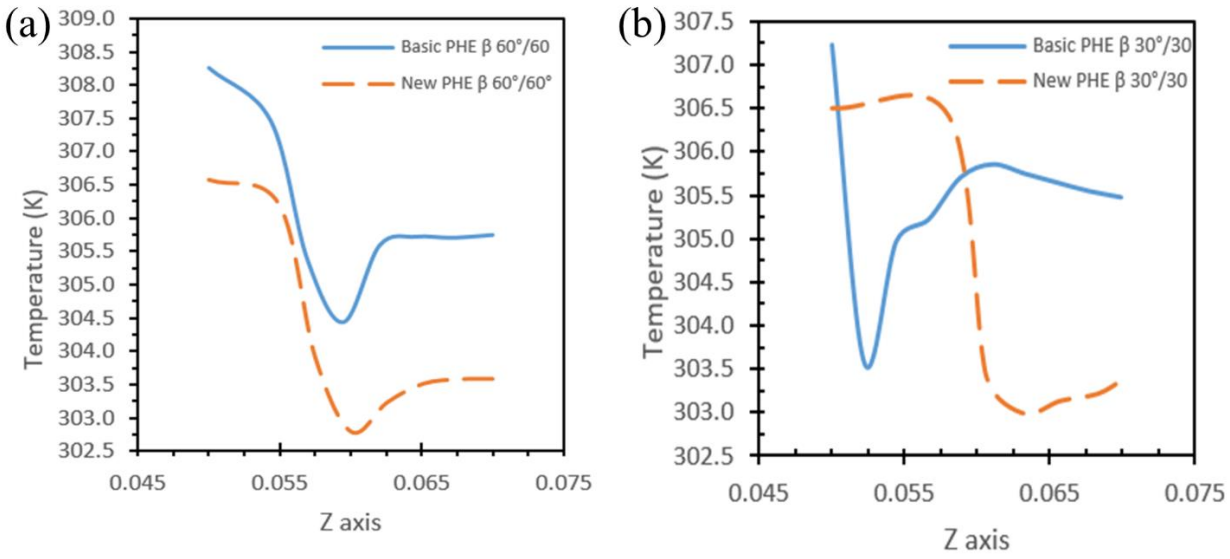

Fig. 15. Temperature profile through the hot channel's outlet axis at $Re = 500$ for basic and new PHEs, (a) $\beta = 60°/60°$, and (b) for $\beta = 30°/30°$.

5.1 Heat transfer correlations

For the present study, classical Sieder [57] empirical correlation (17) was adopted to predicts the Nu correlations. All thermodynamics properties are estimated at the bulk temperature as shown earlier in Eq. (10).

$$Nu = CRe^{p}Pr^{n}\left(\frac{\mu}{\mu_w}\right)^{0.14} \tag{13}$$

In order to find the constant values C and p for each PHE, linear regression technique has been applied to the numerical data in Fig. 5 (a,b). The Pr exponent (n) value ranges from 0.333 up to 0.5 as reported in the literature [19, 20, 58-60]. However, different values for n has already been tested in Alzahrani [22], and 0.333 is found to provide the best approximation. Hence, Nu for the basic and the new PHEs for $\beta = 60°/60°$ is as follows, respectively.

$$Nu = 0.2354\ Re^{0.6415}Pr^{1/3}\left(\frac{\mu}{\mu_w}\right)^{0.14} \tag{18}$$

$$Nu = 0.096\ Re^{0.8273}Pr^{1/3}\left(\frac{\mu}{\mu_w}\right)^{0.14} \tag{19}$$

And Nu for the basic and the new PHEs for $\beta = 30°/30°$ is as follows, respectively.

$$Nu = 0.2332\ Re^{0.6175}Pr^{1/3}\left(\frac{\mu}{\mu_w}\right)^{0.14} \tag{20}$$

$$Nu = 0.1134\, Re^{0.7721} Pr^{1/3} \left(\frac{\mu}{\mu_w}\right)^{0.14} \quad (21)$$

6. Conclusions

Thermal performance of new PHE for symmetric $= 30°/30°$ and $60°/60°$ has been carried out. A comprehensive validation has been performed with a wide range of published experimental and numerical investigations. A realizable $k - \varepsilon$ turbulence model with scalable wall treatment found to provide the most consistent and accurate prediction of the thermal performance of PHE. The numerical simulations have been conducted for steady state single phase (water-water), and counter-current flow arrangement. The CFD results showed that, the thermal performance of the new PHE is significantly higher than that of the well-known PHE. For the newly developed PHE, the calculated Nu is 75% higher than that available for PHE. The ϵ for the new PHE is significantly higher than that of the well-known PHE, and generally exhibits a direct proportional relationship with Re. An empirical correlation for each PHE is developed to estimate Nu values. The newly developed PHE would increase the understanding of the thermal behaviour of the PHE. The findings of the present study could be very useful for many applications, especially for heat recovery applications, where high heat transfer coefficients are required, and for applications where area and weight are limited and require large amount of heat to be removed such as in ships and airplanes. Since the performance of the newly PHE is much higher than the well-known PHE, its size can be further reduced for the same thermal performance allowing for more compact heat exchanger. Further extension of numerical simulations could be performed on the present work to study the difference in the size between the new and the well-known PHE for the same thermal performance.

Acknowledgment

The authors would like to thank the high-performance computing Unit ARCLab, University of Technology Sydney, Australia.

Conflict of Interest

The authors declare no conflict of interest.

References

[1] Cárdenas, B and León, N, "High temperature latent heat thermal energy storage: Phase change materials, design considerations and performance enhancement techniques." *Renewable and sustainable energy reviews*. 27 (2013): 724-737.

[2] Shah, R, "Compact heat exchanger technology and applications." *Heat exchange engineering*. 2 (1991): 1-23.

[3] Shah, R and Webb, R. "Compact and enhanced heat exchangers". in *Heat exchangers—theory and practice. International centre for heat and mass transfer. Symposium. 14*. (1983).

[4] Steinke, ME and Kandlikar, SG. "Single-phase heat transfer enhancement techniques in microchannel and minichannel flows". in *ASME 2004 2nd International Conference on Microchannels and Minichannels*. American Society of Mechanical Engineers. (2004).

[5] Webb, RL. "Advances in modelling of enhanced heat transfer surfaces". in *Institution of Chemical Engineers Symposium Series*. Hemsphere Publishing Corporation. (1994).
[6] Webb, RL and Kim, N-H, "Principles enhanced heat trans." (2004): *Garland Science*.
[7] Zimparov, V, "Energy conservation through heat transfer enhancement techniques." *International Journal of Energy Research*. 26(7) (2002): 675-696.
[8] Webb, R, "Performance evaluation criteria for use of enhanced heat transfer surfaces in heat exchanger design." *International Journal of Heat and Mass Transfer*. 24(4) (1981): 715-726.
[9] Rush, T, Newell, T, and Jacobi, A, "An experimental study of flow and heat transfer in sinusoidal wavy passages." *International journal of heat and mass transfer*. 42(9) (1999): 1541-1553.
[10] Wang, C-C, Lee, C-J, Chang, C-T, and Lin, S-P, "Heat transfer and friction correlation for compact louvered fin-and-tube heat exchangers." *International journal of heat and mass transfer*. 42(11) (1999): 1945-1956.
[11] Wang, C-C, Lee, W-S, and Sheu, W-J, "A comparative study of compact enhanced fin-and-tube heat exchangers." *International Journal of Heat and Mass Transfer*. 44(18) (2001): 3565-3573.
[12] Wen-Jei, Y and Clark, D, "Spray cooling of air-cooled compact heat exchangers." *International Journal of Heat and mass transfer*. 18(2) (1975): 311-317.
[13] Ayub, ZH, "Plate heat exchanger literature survey and new heat transfer and pressure drop correlations for refrigerant evaporators." *Heat Transfer Engineering*. 24(5) (2003): 3-16.
[14] Young, M, "Plate heat exchangers as liquid cooling evaporators in ammonia refrigeration system." *Proceeding of the IIAR 16th Annual Meeting, St Louis* (1994).
[15] Wand, S, "Practical design tips for plate heat exchangers in ammonia refrigerants systems." *Proceeding of the IIAR 16th Annual Meeting, St Louis, Missouri* (1994).
[16] Rao, BP and Das, SK, "An experimental study on the influence of flow maldistribution on the pressure drop across a plate heat exchanger." *Journal of fluids engineering*. 126(4) (2004): 680-691.
[17] Shah, RK and Sekulic, DP, "Fundamentals of heat exchanger design." (2003): *John Wiley & Sons*.
[18] Troupe, R, Morgan, J, and Prifiti, J, "The plate heater versatile chemical engineering tool." *Chemical Engineering Progress*. 56(1) (1960): 124-128.
[19] Okada, K, Ono, M, Tomimura, T, Okuma, T, Konno, H, and Ohtani, S, "Design and heat transfer characteristics of new plate heat exchanger." *Heat Transfer Japanese Research*. 1(1) (1972): 90-95.
[20] Muley, A and Manglik, R, "Experimental study of turbulent flow heat transfer and pressure drop in a plate heat exchanger with chevron plates." *Journal of heat transfer*. 121(1) (1999): 110-117.
[21] Khan, T, Khan, M, Chyu, M-C, and Ayub, Z, "Experimental investigation of single phase convective heat transfer coefficient in a corrugated plate heat exchanger for multiple plate configurations." *Applied Thermal Engineering*. 30(8-9) (2010): 1058-1065.
[22] S. Alzahran, MSI, S. C. Saha,. "A thermo-hydraulic characteristics investigation in corrugated plate heat exchanger". in *Energy Procedia*. Sydney. (2019).
[23] Crozier, R, Booth, J, and Stewart, J, "Heat transfer in plate and frame heat exchangers." *Chemical Engineering Progress*. 60(8) (1964): 43-45.
[24] Emerson, W, "The thermal and hydrodynamic performance of a plate heat exchanger: Flat plates-an apv exchanger-a de lavel exchanger-a rosenblad exchanger." (1967): *National Engineering Laboratory*.

[25] Focke, W, Zachariades, J, and Olivier, I, "The effect of the corrugation inclination angle on the thermohydraulic performance of plate heat exchangers." *International Journal of Heat and Mass Transfer*. 28(8) (1985): 1469-1479.
[26] Gherasim, I, Galanis, N, and Nguyen, CT, "Heat transfer and fluid flow in a plate heat exchanger. Part ii: Assessment of laminar and two-equation turbulent models." *International Journal of Thermal Sciences*. 50(8) (2011): 1499-1511.
[27] Girstmair, J, Zakrzewski, A, Lapraz, F, Handberg-Thorsager, M, Tomancak, P, Pitrone, PG, Simpson, F, and Telford, MJ, "Light-sheet microscopy for everyone? Experience of building an openspim to study flatworm development." *BMC Developmental Biology*. 16 (2016).
[28] Gobble, MM, "News and analysis of the global innovation scene." *Research Technology Management*. 56(5) (2013): 2-8.
[29] Hesselgreaves, J, "The impact of compact heat exchangers on refrigeration technology and cfc replacement". in *ASHRAE-Purdue CFC Conference*. 1990, 500-492.
[30] Kim, MB and Park, CY, "An experimental study on single phase convection heat transfer and pressure drop in two brazed plate heat exchangers with different chevron shapes and hydraulic diameters." *Journal of Mechanical Science and Technology*. 31(5) (2017): 2559-2571.
[31] Talik, AC, "Heat transfer and pressure drop characteristics of a plate heat exchanger". 1995, Texas A&M University.
[32] Thonon, B, Vidil, R, and Marvillet, C, "Recent research and developments in plate heat exchangers." *Journal of Enhanced Heat Transfer*. 2(1-2) (1995).
[33] Vlasogiannis, P, Karagiannis, G, Argyropoulos, P, and Bontozoglou, V, "Air–water two-phase flow and heat transfer in a plate heat exchanger." *International Journal of Multiphase Flow*. 28(5) (2002): 757-772.
[34] Lozano, A, Barreras, F, Fueyo, N, and Santodomingo, S, "The flow in an oil/water plate heat exchanger for the automotive industry." *Applied Thermal Engineering*. 28(10) (2008): 1109-1117.
[35] Kanaris, AG, Mouza, AA, and Paras, SV, "Flow and heat transfer prediction in a corrugated plate heat exchanger using a cfd code." *Chemical Engineering & Technology: Industrial Chemistry-Plant Equipment-Process Engineering-Biotechnology*. 29(8) (2006): 923-930.
[36] Kanaris, A, Mouza, A, and Paras, S, "Flow and heat transfer in narrow channels with corrugated walls: A cfd code application." *Chemical Engineering Research and Design*. 83(5) (2005): 460-468.
[37] Tsai, Y-C, Liu, F-B, and Shen, P-T, "Investigations of the pressure drop and flow distribution in a chevron-type plate heat exchanger." *International communications in heat and mass transfer*. 36(6) (2009): 574-578.
[38] Bassiouny, M and Martin, H, "Flow distribution and pressure drop in plate heat exchangers—ii z-type arrangement." *Chemical Engineering Science*. 39(4) (1984): 701-704.
[39] Bassiouny, M and Martin, H, "Flow distribution and pressure drop in plate heat exchangers—i u-type arrangement." *Chemical Engineering Science*. 39(4) (1984): 693-700.
[40] Asif, M, Aftab, H, Syed, H, Ali, M, and Muizz, P, "Simulation of corrugated plate heat exchanger for heat and flow analysis." *International Journal of Heat and Technology*. 35(1) (2017): 205-210.
[41] Elshafei, E, Awad, M, El-Negiry, E, and Ali, A, "Heat transfer and pressure drop in corrugated channels." *Energy*. 35(1) (2010): 101-110.

[42] Dewan, A, Mahanta, P, Raju, KS, and Kumar, PS, "Review of passive heat transfer augmentation techniques." *Proceedings of the Institution of Mechanical Engineers, Part A: Journal of Power and Energy*. 218(7) (2004): 509-527.
[43] Gugulothu, R, Reddy, KVK, Somanchi, NS, and Adithya, EL, "A review on enhancement of heat transfer techniques." *Materials Today: Proceedings*. 4(2) (2017): 1051-1056.
[44] Jain, S, Joshi, A, and Bansal, P, "A new approach to numerical simulation of small sized plate heat exchangers with chevron plates." *Journal of Heat Transfer*. 129(3) (2007): 291-297.
[45] "Fluent 6.3 user manual, access date 13.11.2018 (https://www.Sharcnet.Ca/software/fluent6/html/ug/main_pre.Htm)."
[46] Menter, F and Esch, T. "Elements of industrial heat transfer predictions". in *16th Brazilian Congress of Mechanical Engineering (COBEM)*. sn. (2001).
[47] Wilcox, DC, "Formulation of the kw turbulence model revisited." *AIAA journal*. 46(11) (2008): 2823-2838.
[48] Borouchaki, H, George, PL, Hecht, F, Laug, P, and Saltel, E, "Delaunay mesh generation governed by metric specifications. Part i. Algorithms." *Finite elements in analysis and design*. 25(1-2) (1997): 61-83.
[49] Gherasim, I, Taws, M, Galanis, N, and Nguyen, CT, "Heat transfer and fluid flow in a plate heat exchanger part i. Experimental investigation." *International Journal of Thermal Sciences*. 50(8) (2011): 1492-1498.
[50] Thonon, B. "Design method for plate evaporators and condensers". in *BHR Group Conference Series Publication*. Mechanical Engineering Publications Limited. (1995).
[51] Lee, J and Lee, K-S, "Flow characteristics and thermal performance in chevron type plate heat exchangers." *International Journal of Heat and Mass Transfer*. 78 (2014): 699-706.
[52] Cieśliński, JT, Fiuk, A, Typiński, K, and Siemieńczuk, B, "Heat transfer in plate heat exchanger channels: Experimental validation of selected correlation equations." *Archives of Thermodynamics*. 37(3) (2016): 19-29.
[53] Sparrow, E and Hossfeld, L, "Effect of rounding of protruding edges on heat transfer and pressure drop in a duct." *International Journal of Heat and Mass Transfer*. 27(10) (1984): 1715-1723.
[54] Blomerius, H and Mitra, N, "Numerical investigation of convective heat transfer and pressure drop in wavy ducts." *Numerical Heat Transfer: Part A: Applications*. 37(1) (2000): 37-54.
[55] Won, S and Ligrani, P, "Comparisons of flow structure and local nusselt numbers in channels with parallel-and crossed-rib turbulators." *International journal of heat and mass transfer*. 47(8-9) (2004): 1573-1586.
[56] Focke, W and Knibbe, P, "Flow visualization in parallel-plate ducts with corrugated walls." *Journal of Fluid Mechanics*. 165 (1986): 73-77.
[57] Sieder, EN and Tate, GE, "Heat transfer and pressure drop of liquids in tubes." *Industrial & Engineering Chemistry*. 28(12) (1936): 1429-1435.
[58] Longo, G and Gasparella, A, "Refrigerant r134a vaporisation heat transfer and pressure drop inside a small brazed plate heat exchanger." *International journal of refrigeration*. 30(5) (2007): 821-830.
[59] Talik, A, Fletcher, L, Anand, N, and Swanson, L, "Heat transfer and pressure drop characteristics of a plate heat exchanger using a propylene-glycol/water mixture as the working fluid". 1995, American Society of Mechanical Engineers, New York, NY (United States).

[60] Wanniarachchi, A, Ratnam, U, Tilton, B, and Dutta-Roy, K, "Approximate correlations for chevron-type plate heat exchangers". 1995, American Society of Mechanical Engineers, New York, NY (United States).